



1 **Biogeochemical and biophysical responses to episodes of wildfire smoke from**
2 **natural ecosystems in southwestern British Columbia, Canada**

3
4 Sung-Ching Lee¹, Sara H. Knox¹, Ian McKendry¹, T. Andrew Black²

5
6 ¹Department of Geography, University of British Columbia, Vancouver, Canada

7 ²Faculty of Land and Food Systems, University of British Columbia, Vancouver,
8 Canada

9
10 **Correspondence:** Sung-Ching Lee (sungching.lee@geog.ubc.ca)

11
12 **Abstract**

13 Area burned, number of fires, seasonal fire severity, and fire season length are all
14 expected to increase in Canada, with largely unquantified ecosystem feedbacks.
15 However, there are few observational studies measuring the ecosystem-scale
16 biogeochemical and biophysical properties during smoke episodes, and hence
17 accessing productivity effects of changes in incident diffuse photosynthetically active
18 radiation (PAR). In this study, we leverage two long-term eddy covariance
19 measurement sites in forest and wetland to study four smoke episodes, which
20 happened at different times and differed in length, over four different years. We found
21 that the highest decrease of shortwave irradiance due to smoke was about 50% in July
22 and August but increased to about 90% when the smoke arrived in September. When
23 the smoke arrived in the later stage of summer, impacts on *H* and *LE* were also
24 greatest. Smoke generally increased the diffuse fraction from ~0.30 to ~0.50 and
25 turned both sites into stronger carbon-dioxide (CO₂) sinks with increased productivity
26 of ~18% and ~7% at the forest and wetland sites, respectively. However, when the
27 diffuse fraction exceeded 0.80 as a result of dense smoke, both ecosystems became
28 CO₂ sources as total PAR dropped to low values. The results suggest that this kind of
29 natural experiment is important for validating future predictions of smoke-
30 productivity feedbacks.

31
32
33 **1 Introduction**

34 Among the many ecosystem services provided by temperate forests and wetlands in
35 western North America, climate regulation is identified as one of their most important
36 benefits to society (Millennium Ecosystem Assessment, 2005). However, these
37 services are being greatly altered by increasing wildfire occurrences, both in terms of
38 frequency and duration (Settele et al., 2015). In addition to affecting visibility and air



39 quality, aerosols arising from biomass burning can alter the radiation budget by
40 scattering and absorbing radiation and hence potentially influence cloud processes
41 (Crutzen & Andreae, 1990). The overall effect of aerosols on climate still remains
42 uncertain according to the latest IPCC assessment (Pachauri et al., 2014). This has
43 triggered enormous interest in the radiative impacts of smoke plumes induced by
44 biomass burning (Chubarova et al., 2012; Lasslop et al., 2019; Markowicz et al.,
45 2017; McKendry et al., 2019; Moreira et al., 2017; Oris et al., 2014; Park et al., 2018;
46 Sena et al., 2013). Heavy smoke conditions were found to cause net surface cooling of
47 3 °C in Amazonia (Yu et al., 2002), while some have observed net radiative cooling at
48 the surface and net radiative warming at the top of the atmosphere in the Arctic and
49 southeastern United States (Markowicz et al., 2017; Taubman et al., 2004), resulting
50 in enhanced atmospheric stability. It has been estimated that aerosol emissions from
51 boreal fires might have a net effect of inducing a positive feedback to global warming
52 (Oris et al., 2014). Jacobson (2014) also suggested a net global warming of 0.4 K by
53 including black and brown atmospheric carbon, heat and moisture fluxes, and cloud
54 absorption effects. However, other studies using atmospheric modelling found a net
55 cooling effect of aerosols, which can lead to a net reduction in the global radiative
56 forcing of fires (Landry et al., 2015; Ward et al., 2012).

57 Changes in solar irradiance, in particular photosynthetically active radiation
58 (PAR, 400–700 nm), affect plant physiological mechanisms that influence
59 photosynthesis (i.e., gross primary production (GPP)), net ecosystem exchange of
60 CO₂ (NEE), and light use efficiency (LUE). Sub-canopy leaves, especially in forest
61 ecosystems, typically remain under light-deficit conditions. Increasing diffuse
62 radiation makes it easier for PAR photons to penetrate deeper into the canopy
63 (Doughty et al., 2010; Kanniah et al., 2012; Knohl and Baldocchi, 2008; Rap et al.,
64 2015). Additionally, diffuse PAR coming from different angles can increase the
65 efficiency of CO₂ assimilated by plants because leaves are generally at different
66 orientations (Alton et al., 2006). This increase in photosynthesis that results from the
67 trade-off between decreased solar radiation and increased PAR scattering is referred
68 to as the diffuse radiation fertilization (DRF) effect (Moreira et al., 2017; Park et al.,
69 2018; Rap et al., 2015). However, DRF has not always been observed under fire
70 smoke conditions and appears to be ecosystem-dependent. For instance, Ezhova et al.,
71 (2018) found that the mechanisms causing the increases in GPP are different between
72 the boreal coniferous and mixed forest ecosystems. Some studies suggest that DRF
73 might depend on canopy height and the leaf area index (LAI) (Cheng et al., 2015;
74 Kanniah et al., 2012; Niyogi et al., 2004). For example, Cheng et al. (2015) found an
75 increase in GPP due to diffuse radiation for forest sites but not for cropland sites using
76 AmeriFlux data from ten temperate climate ecosystems including three forests and



77 seven croplands. Therefore, it is still uncertain how the changes in diffuse radiation
78 affect GPP and it is also not clear how large the effect of aerosols is on diffuse
79 radiation.

80 With an area of 95 million hectares (Ministry of Forests, 2003), British Columbia
81 (BC), Canada, is almost double the size of California, USA. Of that area, almost 64%
82 is forested with less than one-third of one percent of BC's forest land harvested
83 annually (Ministry of Forests, Mines and Land, 2010). Wetlands in BC comprise
84 around 5.28 million hectares or approximately 5% of the land base (Wetland
85 Stewardship Partnership, 2009). Therefore, responses of forests and wetlands to
86 wildfire smoke are very likely to have a significant impact on regional carbon
87 budgets. In western Canada, a previous study found that a short, but severe, wildfire
88 smoke episode in 2015 appreciably changed the energy balance and net CO₂ exchange
89 at wetland and forest sites in southwestern BC (McKendry et al., 2019). Another
90 study investigated 2017 and 2018 smoke events in southwestern BC and found that
91 the aerosols from wildfires suppressed the development of deep mountain convective
92 layers, and hence inhibited vertical mixing, convection and cloud development
93 (Ferrara et al., 2020). It is unclear whether the changes in NEE found by McKendry et
94 al. (2019) were due to changes in GPP or ecosystem respiration (R_e). Furthermore,
95 biogeochemical and biophysical properties of wetland and forest ecosystems might
96 respond differently to smoke events with different intensities and durations. In 2015,
97 2017, 2018, and 2020, southwestern BC experienced smoke episodes that differed in
98 both duration and intensity.

99 In this study, we investigate the effect of those fire events on two natural
100 ecosystems in southwestern BC; one is a temperate forest ecosystem (Douglas-fir,
101 *Pseudotsuga menziesii*) and the other is a wetland ecosystem (restored peatland) (Fig.
102 1). We aim to provide a better understand of biogeochemical and biophysical
103 responses to wildfire smoke episodes in natural ecosystems in southwestern BC.
104 Specifically, we aim to (1) evaluate smoke-induced changes in shortwave irradiance,
105 albedo, and energy partitioning at the two sites, (2) assess the biogeochemical
106 responses to smoke by investigating GPP and R_e at the two sites, and (3) estimate the
107 maximum effect of smoke on GPP due to changes in the ratio of diffuse to total PAR.
108 Ultimately, we hope to provide a firm foundation for upscaling the impacts of wildfire
109 smoke on the regional CO₂ budget.



110 **2 Methodology**

111 **2.1 Wildfire smoke episodes**

112 **2.1.1 Overview**

113 In 2015, there were a series of wildfires across different provinces in Canada. During
114 4–8 July 2015, smoke spread across most of North America and a particularly intense
115 event occurring in ~150 km north of Vancouver seriously impacted air quality and
116 visibility in southwestern BC. The detailed evolution and synoptic patterns associated
117 with this event are described in McKendry et al. (2019). In summer 2017, a smoke
118 haze settled over the BC coast due to offshore winds advecting smoke from wildfires
119 in the BC Interior. The wildfire season in 2018 eclipsed the previous year's as the
120 worst recorded in BC history with 2,117 fires consuming 1,354,284 hectares of land.
121 ([https://www2.gov.bc.ca/gov/content/safety/wildfire-status/about-bcws/wildfire-
122 history/wildfire-season-summary](https://www2.gov.bc.ca/gov/content/safety/wildfire-status/about-bcws/wildfire-
122 history/wildfire-season-summary)). Smoke covered the BC coast area for
123 approximately 20 days with additional plumes drifting north from similar fires in
124 Washington state, USA. In 2020, BC recorded a quiet fire season with 637 wildfires
125 burning just over 15,000 hectares of land between 1 April and 1 October. However,
126 southwestern BC was significantly affected by smoke advected northward from an
127 intense fire season affecting Washington state, Oregon, and California, USA. Notably,
128 the cross-border smoke arrived in September, somewhat later than usual.
129



130

131 **Figure 1.** Locations of the all sites mentioned in text. Observations of aerosol optical
132 depth at the reference 500 nm wavelength (AOD_{500}) and particulate matter less than
133 $2.5 \mu\text{m}$ in diameter ($PM_{2.5}$) were collected at Saturna Island AERONET site and
134 Vancouver International Airport, respectively. Flux and climate data of wetland and
135 forest ecosystems were measured at Burns Bog and Buckley Bay, respectively.



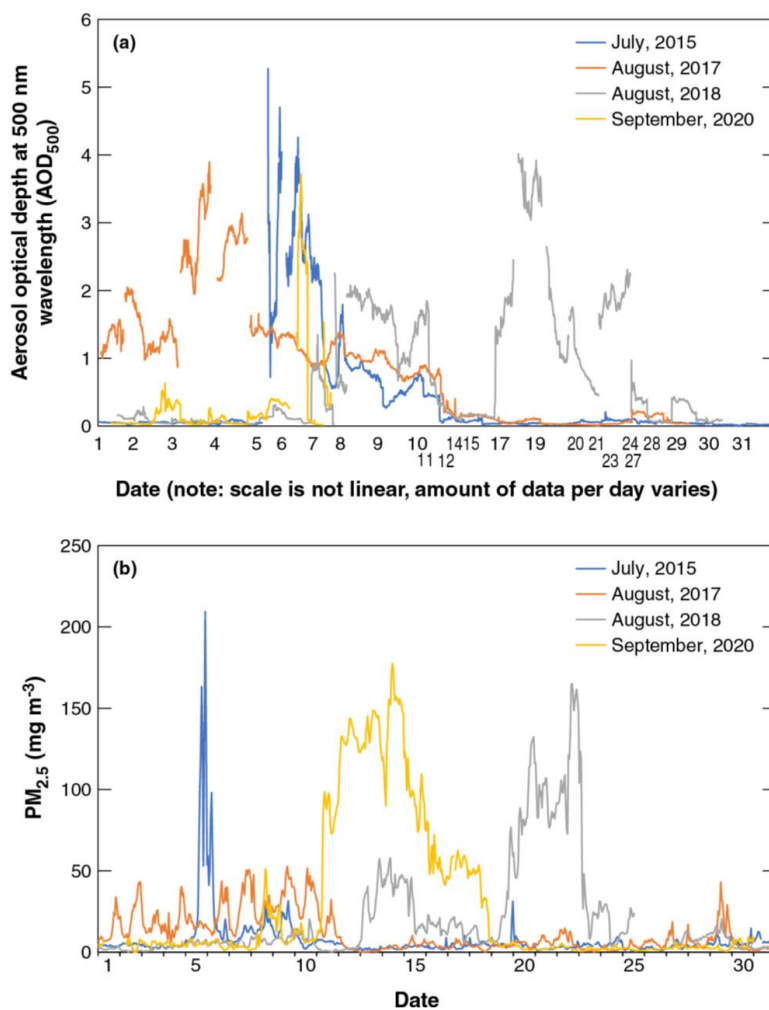
136 **2.1.2 AERONET and AEROCAN**

137 The global AERONET (AErosol RObotic NETwork) has been in operation since 1993
138 and is focused on measurements of vertically integrated aerosol properties using the
139 CIMEL sunphotometer/sky radiometer instrument (Holben et al., 1998). AEROCAN
140 CIMELs (AEROCAN is the Canadian sub-network of AERONET) include a facility
141 on Saturna Island, which is located 55 km to the south of the city of Vancouver (Fig.
142 1). Here, solar irradiance is acquired across eight spectral channels (340, 380, 440, 500,
143 670, 870, 1020 and 1640 nm) that are transformed into three processing levels of
144 aerosol optical depth (AOD); 1.0 – non-cloud screened; 1.5 – cloud screened; and 2.0
145 – cloud screened and quality assured. McKendry et al. (2011) demonstrated the
146 application of these data to the transport of California wildfire plumes. In this paper,
147 we present the level 1.5 AOD data at the reference 500 nm wavelength in order to
148 compare both the magnitude and duration of the four smoke episodes.

149 The monthly course of AOD₅₀₀ for each of four episodes at Saturna Island is
150 shown in Fig. 2a. For each event there were persistent multi-day periods when
151 AOD₅₀₀ > 2 and reached or exceeded a value of 4. The impact of smoke events on
152 ground level PM_{2.5} (particulate matter less than 2.5 µm in diameter) concentrations at
153 Vancouver International Airport is shown in Fig. 2b. From Fig. 2, it is evident that the
154 event of 2015, although the shortest of the four events, was the most intense with both
155 AOD₅₀₀ > 5 and ground level PM_{2.5} concentrations > 200 µg m⁻³, exceeding those of
156 the other three events. This is likely due to the close proximity of the fires in this case
157 (McKendry et al. 2019). The event of August 2017 was of somewhat longer duration
158 in which AOD₅₀₀ peaked at 4 but ground level concentrations remained comparatively
159 low (< 50 µg m⁻³) and showed a strong diurnal pattern associated with boundary layer
160 entrainment from elevated layers (Ferrara et al. 2020). In August 2018 the smoke was
161 persistent and included a double maximum. Ground level PM_{2.5} concentrations
162 exceeded 150 µg m⁻³ and AOD₅₀₀ reached 4. Finally, the early fall event in September
163 2020 was also a persistent event in which ground level concentrations exceeded 150
164 µg m⁻³ and AOD₅₀₀ reached 4. There was evidence in this case of two short peaks in
165 smoke in late September that followed the main event.

166 In summary, the four events were all quite different with respect to intensity of
167 smoke, duration, and impact at ground level (a function of transport height of smoke
168 layers and boundary layer processes). The most similar in character appear to be the
169 2018 and 2020 events, although it is likely that the “age” and life history of smoke
170 was different for these two cases due to the different geographical sources and
171 distance travelled.

172



173
174 **Figure 2.** (a) AOD₅₀₀ at Saturna Island and (b) PM_{2.5} observations at Vancouver
175 International Airport for the four months with wildfire smoke in Vancouver, British
176 Columbia, Canada. There are different numbers of AOD₅₀₀ data points per day in
177 panel a and 24 PM_{2.5} data points per day in panel b.
178



179 2.1.3 Study periods

180 Study periods were defined using the following criteria. First, days were selected with
181 $AOD_{500} > 0.5$ or $PM_{2.5} > 50 \mu\text{g m}^{-3}$. Second, Hazard Mapping System Fire and Smoke
182 Product from The Office of Satellite and Product Operations at the National Oceanic
183 and Atmospheric Administration were used to plot smoke polygons over the
184 southwestern British Columbia region. In the final step, we included a day into the study
185 periods when the two sites were covered by the smoke polygon classified in the medium
186 category. The study periods during the four months with wildfire smoke and the
187 respective maximum AOD_{500} and $PM_{2.5}$ values are summarized in Table 1.

188

189 **Table 1.** Summaries for the four study periods.

Year	Study period	Maximum AOD_{500}	Maximum $PM_{2.5}$ ($\mu\text{g m}^{-3}$)
2015	4–8 July	5.3	210
2017	1–11 August	3.9	53
2018	8–23 August	4.0	165
2020	8–18 September	3.7*	178

190 *There were no available observations during the 2020 smoke episode. The value
191 shown here was observed on 6 September 2020.

192

193 2.2 Radiative and turbulent flux measurements

194 2.2.1 Wetland site

195 The rewetted peatland site (AmeriFlux ID: CA-DBB, $122^{\circ}59'5.60''$ W, $49^{\circ}07'45.59''$
196 N) (Christen & Knox, 2021) is located in the centre of the Burns Bog Ecological
197 Conservancy Area in British Columbia, Canada (Fig. 1). Burns Bog is recognized as
198 the largest raised bog ecosystem on the west coast of Canada (Christen et al., 2016).
199 The 5-m-tall flux tower at Burns Bog was built in 2014 equipped with an eddy
200 covariance (EC) system to continuously measure turbulent fluxes of sensible heat (H),
201 latent heat (LE), and carbon-dioxide (F_{CO_2}). F_{CO_2} and the heat fluxes were computed
202 using the 30-min covariance of turbulent fluctuations in vertical wind speed and scalar
203 of interest and standard quality control involved removing spikes was applied to half-
204 hourly EC-measured fluxes. We applied block averaging and time-lag removal by
205 covariance maximization (Moncrieff et al., 1997). Coordinate rotations were
206 performed so that mean wind speeds at each 30-min averaging interval were zero in
207 the cross-wind and vertical directions. The flux data were further filtered to exclude
208 the errors indicated by the sonic anemometer and IRGA diagnostic flags, typically
209 attributable to heavy rainfall or snowfall. Fluxes were also filtered for spikes in 30-
210 min mean mixing ratios, variances and covariances with thresholds. F_{CO_2} was
211 corrected by adding the estimated rate of change in CO_2 storage in the air column



212 below the EC sensor height to obtain NEE (Hollinger et al., 1994; Morgenstern et al.,
213 2004). After obtaining cleaned heat fluxes, we filtered NEE and heat fluxes with low
214 friction velocity (u_*). The u_* threshold was 0.03 m s^{-1} determined by using moving
215 point test (Papale et al., 2006). The algorithm used for u_* threshold detection was run
216 in R (R Core Team, 2017) by using the REddyProc 1.2-2 R package (Wutzler et al.,
217 2018). NEE was partitioned into GPP and R_e using a nighttime-based partitioning
218 method (Reichstein et al., 2005). Four components of radiation (shortwave, longwave,
219 incoming, and outgoing) were continuously measured by a four-component net
220 radiometer (CNR1, Kipp and Zonen, Delft, Holland) on top of the tower. The surface
221 albedo (α) of the site, i.e., the ratio of the reflected shortwave radiation (K_{\uparrow}) to the
222 shortwave irradiance (K_{\downarrow}), was measured at noon. Several climate variables were also
223 measured (e.g., net radiation (R_n), relative humidity (RH), and water table level).
224 Further details of the site are described in Christen et al. (2016), Lee et al. (2017), and
225 D'Acunha et al. (2019).

226

227 2.2.2 Forest site

228 Buckley Bay (AmeriFlux ID: CA-Ca3) is a flux tower with EC and radiation sensors
229 measuring exchanges between a coniferous forest stand (Douglas-fir, 27 years old)
230 and the atmosphere (Black, 2021). The site is located on the eastern slopes of the
231 Vancouver Island Range, about 150 km to the west of Vancouver (Fig. 1). A 21-m-
232 tall, 25-cm triangular open-lattice flux tower was erected in 2001 and equipped with
233 an EC system to continuously measure turbulent fluxes of H , LE , and F_{CO_2}
234 (Humphreys et al., 2006). In November 2017, this tower was decommissioned, and in
235 June 2017, a 33-m-tall walk-up scaffold flux tower (2 m wide x 4 m long) was erected
236 and equipped with an EC system to continuously measure H , LE , and F_{CO_2} . H , LE ,
237 and F_{CO_2} were calculated and F_{CO_2} was also corrected by adding the estimated rate of
238 change in CO_2 storage in the air column below the EC sensor height to obtain NEE
239 (Hollinger et al., 1994; Morgenstern et al., 2004). Fluxes during low turbulence
240 periods (friction velocity, u_* , less than 0.16 m s^{-1}) were rejected (Lee et al., 2020a).
241 NEE was partitioned into GPP and R_e using a nighttime relationship model following
242 the Fluxnet-Canada Research Network procedure (Barr et al., 2004; Chen et al.,
243 2009). Four components of radiation were continuously measured by a CNR1 (Kipp
244 and Zonen) at the 32-m height facing south. α was calculated as $K_{\downarrow}/K_{\uparrow}$ at noon as for
245 the wetland site. The diffuse fraction of PAR was measured at the 32-m height facing
246 south (Sunshine sensor type BF3, Delta-T Devices Ltd, Cambridge, UK). Information
247 of quantum sensor is described in the next section. Further details of the site are
248 described in Jassal et al. (2009), Krishnan et al. (2009), and Lee et al. (2020b).



249 **2.3 Diffuse photosynthetically active radiation and light use efficiency**

250 As mentioned above, it has been found that the dependence of GPP on the fraction of
251 diffuse PAR (called “diffuse fraction” hereafter) is ecosystem dependent. In this
252 study, we estimated the maximum GPP increase using the relationship between
253 ecosystem light use efficiency (LUE) and diffuse fraction, as well as the relationship
254 between PAR and diffuse fraction. First, cloudy conditions increase incident diffuse
255 radiation but also decrease total radiation (direct plus diffuse), which can counteract
256 productivity increases due to diffuse radiation alone (Alton, 2008; Letts et al., 2005;
257 Oliphant et al., 2011). Cloudy conditions also affect other meteorological drivers of
258 photosynthesis such as vapor pressure deficit (VPD) and surface temperature that
259 regulate stomatal conductance and can confound quantification of the photosynthetic
260 response to diffuse fraction (Strada et al., 2015). In order to exclude this, we only
261 included the day that was just before or just after the study periods if it was sunny.
262 Extraterrestrial solar radiation (K_{ext}), the flux density of solar radiation at the outer
263 edge of atmosphere, was also calculated using date, time, and latitude at the sites to
264 obtain atmospheric bulk transmissivity ($T = K_d/K_{ext}$), and hence determine whether a
265 day was sunny ($T > 0.65$).

266 Second, as there was no diffuse PAR measurement at the Burns Bog site, the
267 formula (diffuse fraction = $1.45 - 1.81T$) following Gu et al. (2002) and Alton (2008)
268 was used to estimate the diffuse fraction for this site. Also, diffuse fraction was set at
269 0.95 when T was less than 0.28 and at 0.10 when T was greater than 0.75. The diffuse
270 fraction at the Buckley Bay site in 2015 was estimated using the same method
271 because diffuse PAR measurement was not available yet. For the later three episodes,
272 the diffuse fraction was calculated as the diffuse PAR (PAR_d) measured by the BF3
273 divided by the incoming total PAR (PAR_g) measured by the quantum sensor.

274 Following Cheng et al. (2016), LUE ($\mu\text{mol CO}_2 (\mu\text{mol photon})^{-1}$) was defined as
275 the ratio of mean daily GPP ($\mu\text{mol m}^{-2} \text{s}^{-1}$) to mean daily PAR_g ($\mu\text{mol m}^{-2} \text{s}^{-1}$), which
276 gives $GPP = LUE \times PAR_g$. One important note, LUE is defined as GPP per unit
277 absorbed PAR_g (i.e. $APAR = fAPAR \times PAR_g$), where $fAPAR$ is the fraction of the
278 absorbed PAR_g . Generally, $fAPAR$ is affected by leaf area index (LAI), the solar
279 zenith angle, and other factors such as leaf color (Ezhova et al., 2018). Typically,
280 $fAPAR$ for tree heights greater than 10 m and at a moderate zenith angle (i.e., $40-60^\circ$)
281 can be estimated to be between 0.8 and 0.9 (Hovi et al., 2016).

282



283 **3 Results**

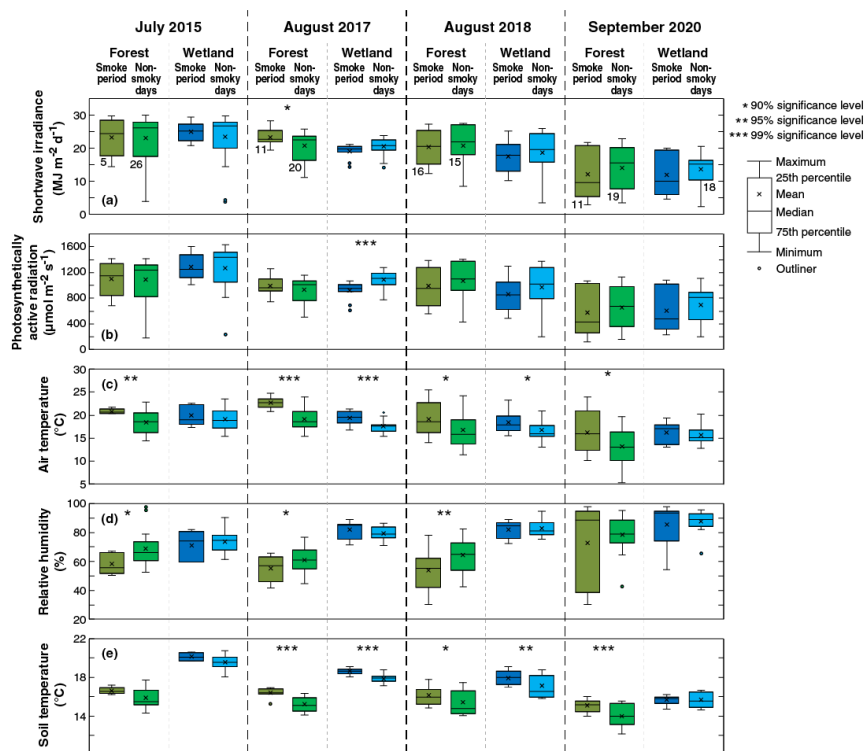
284 **3.1 Radiative changes and biophysical responses**

285 **3.1.1 Radiation and environmental conditions**

286 Fig. 3 shows boxplots for measured K_d , PAR_g , air temperature (T_a), RH, and soil
287 temperature (T_s) during the smoky days (as defined in Table 1) and non-smoky days
288 (defined as all the remaining days in the same month) over the study periods. The
289 boxplot shows the mean, median, interquartile range, and outlier values. Tests of
290 significance are also shown in Figs. 3 and 4 to indicate when differences between the
291 smoky and non-smoky days are statistically significant and at what significance level
292 (Students T tests). During days that were not affected by smoke, both sites
293 experienced a smooth diurnal course of radiation components consistent with typical
294 summer clear-sky conditions. Mean K_d values were generally lower during the
295 smoke events compared to the days that were not affected by smoke (Fig. 3), but these
296 differences were not statistically significant with the exception of the August 2017
297 event at Buckley Bay. The difference was much greater for the September 2020 case.
298 A few low K_d values were observed during those non-smoky days and were likely
299 due to the rain events (Fig. S1). On clear-sky days, mean daily T values were
300 approximately 70% at the two sites except during 2020 when it was ~60% (Fig. 4).
301 The mean T values during the smoky days typically dropped to ~60% but decreased to
302 ~40% in 2020 (Fig. 4). In 2015, the most dramatic impact of the smoke plume on K_d
303 occurred on 5 July at Buckley Bay and 6 July at Burns Bog, respectively, during
304 otherwise clear sky conditions (Fig. S2). The mean daily T dropped to ~35% and
305 ~50% at Buckley Bay and at Burns Bog, respectively (Fig. S3). During the summer in
306 2017, the wetland site experienced the biggest impact of smoke on 4 August when T
307 decreased to ~40% (Fig. S3). One day later, on 6 August, the forest site was most
308 affected by the smoke with T reduced to ~50% (Fig. S3). The longest duration smoke
309 episode of the four occurred in 2018, and reduced T much earlier at Buckley Bay (11
310 August) than at Burns Bog (19 August). The magnitudes of the decrease in T were
311 similar at the two sites (dropped to ~35%) in 2018 (Fig. S3). The September 2020
312 case is notable for being the latest (season-wise) of the four cases, and the only case in
313 which K_d was reduced below 10 W m^{-2} at both sites (Fig. S2). Mean daily T values in
314 September were about 70% at the two sites under sunny days (Fig. S3). T decreased
315 appreciably to ~10% and 20% at Buckley Bay and at Burns Bog, respectively, due to
316 the smoke. These were the lowest values among the four study periods. Both T_a and T_s
317 were higher during the smoky days than non-smoky days (Fig. 2) and the differences
318 were mostly statistically significant. T_s experienced smaller changes compared to T_a .
319 RH dropped at the forest site during the smoke events except the 2020 case. In
320 contrast, the wetland site had higher RH when affected by wildfire smoke but the



321 changes were not statistically significant. This partially reflects the substantial
 322 difference in wetness between the two sites.
 323



324
 325 **Figure 3.** Box plots of shortwave irradiance, average of photosynthetically active
 326 radiation during daytime, daily average of air temperature, daily average of relative
 327 humidity, and daily average of soil temperature over the study periods and other days,
 328 respectively, in 2015, 2017, 2018, and 2020 at Buckley Bay (the forest site) and at
 329 Burns Bog (the peatland site). The numbers of daily cases (n) used in the significance
 330 tests for each period for both the forest and wetland sites are shown beneath the
 331 boxplot pairs for the forest site in panel a. Unless otherwise shown, n is the same for
 332 all other variables and boxplot pairs in the same year.
 333



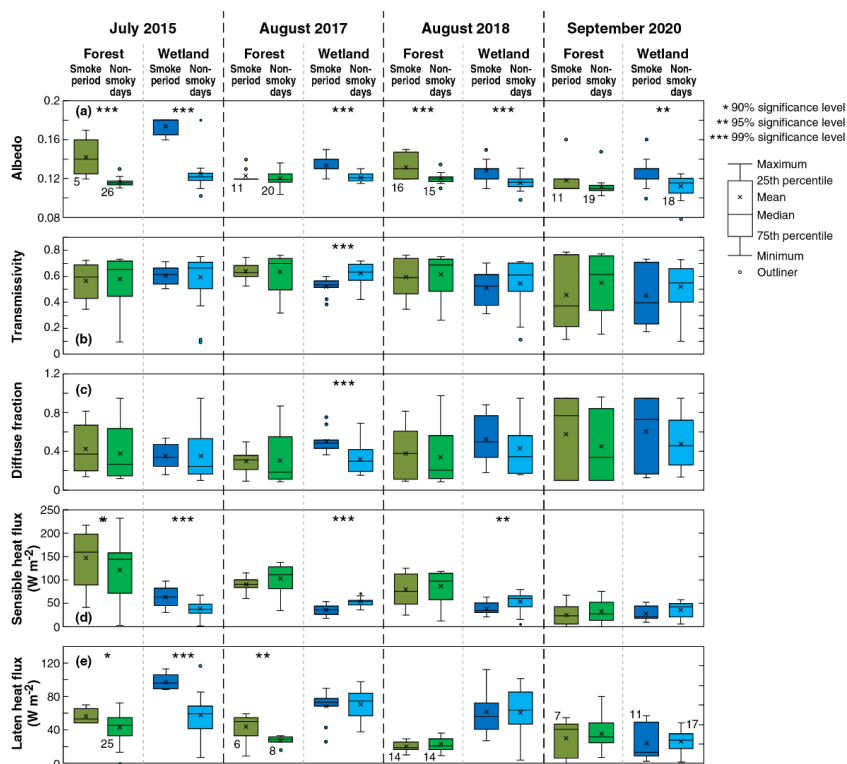
334 3.1.2 Albedo and energy partitioning

335 Under non-smoky conditions, mean albedo values were 0.12 and 0.13 at Buckley Bay
336 and Burns Bog, respectively (Fig. 4). These relatively low values are expected as the
337 forest site has taller vegetation that will trap light more effectively, while the wetland
338 site has dark water surfaces that lead to a lower albedo. A slight increase in albedo
339 was observed at both sites with the arrival of smoke during the four study periods and
340 the increases were mostly statistically significant. In 2015, the albedo increased more
341 than the other three years, especially at the wetland site. Excluding the 2015 case, the
342 increase in albedo was only ~ 10% at both sites.

343 The changes in H and LE during the smoky days were different every year
344 compared to the non-smoky days (Fig. 4). Cloud conditions could play a role in
345 determining magnitudes of H and LE . Thus, the mean daytime time values of H and
346 LE are also shown in Fig. S3. As with K_d in 2015, the most significant impact on H
347 was on 5 July at Buckley Bay and Burns Bog, where H decreased to 18% and 45%
348 respectively of non-smoky mean daytime ($PAR_g \geq 20 \mu\text{mol m}^{-2} \text{s}^{-1}$) values. The
349 impacts on LE were less than for H at both sites, with the minimum for LE occurring
350 on 9 July. At both sites, the Bowen ratio, β ($= H/LE$) was appreciably reduced on 5
351 July, with the greater reduction at Buckley Bay (i.e., from 3.22 to 0.84) due to the
352 large reduction in H . In 2017, the smallest decrease in H , which maintained at 45% of
353 non-smoky mean daytime time values, was found for Buckley Bay among the four
354 study periods. However, LE dropped appreciably at Buckley Bay (14% of non-smoky
355 mean daytime time values). During the 2018 smoke episode, Buckley Bay showed a
356 similar response in H as 2015 but LE still decreased more than 2015. During 2017 and
357 2018 smoke events, H and LE had a similar response at Burns Bog. H decreased to
358 32% and 34% of non-smoky mean daytime time values in 2017 and 2018,
359 respectively, while LE decreased to 27% and 34% of non-smoky mean daytime time
360 values, respectively, but the differences in LE were not statistically significant. In
361 September 2020, the latest of the four smoke episodes, H and LE dropped below 5
362 and 10 W m^{-2} at Buckley Bay and Burns Bog, respectively.

363 In summary, the forest site had higher H than the wetland site during the smoky
364 days, except for the 2020 case (Fig. 4). LE was maintained at a higher value at the
365 wetter site (Burns Bog) compared to the forest site during smoke conditions. Due to
366 the smaller changes in H and LE , β at Burns Bog stayed near 50% of non-smoky
367 mean daytime time values. However, β at Buckley Bay responded much more
368 dramatically and the observed range of β was between 26 and 90% of non-smoky
369 mean daytime time values.

370



371
 372 **Figure 4.** Box plots of albedo at noon, daily average of transmissivity, daily average
 373 of diffuse fraction, daily average of sensible heat flux, and daily average of latent heat
 374 flux at the forest and wetland sites during the smoke events and non-smoky days,
 375 respectively, in 2015, 2017, 2018, and 2020. The numbers of daily cases (n) used in
 376 the significance tests for each period for both the forest and wetland sites are shown
 377 beneath the boxplot pairs for the forest site in panel a. Unless otherwise shown, n is
 378 the same for all other variables and boxplot pairs in the same year.
 379



380 **3.1.3 Diffuse radiation fraction**

381 Fig. 4 shows the diffuse fraction (mean daily PAR_d / mean daily PAR_g) during the
382 four smoke episodes at Buckley Bay. Under non-smoky conditions over the four
383 years, PAR_d is roughly a constant fraction of PAR_g (i.e., 0.30). With the arrival of
384 smoke in July or August, the diffuse fraction increased to about 0.40. When the
385 smoke arrived later in the season, as in September 2020, the diffuse fraction increased
386 significantly to almost 0.80. There was another peak in diffuse fraction on 23
387 September 2020 (Fig. S3). We attribute this to intermittent transport events linked to
388 the original smoke episode. Over the four study periods, mean daily PAR_g values
389 decreased during the smoke events (Fig. 3), suggesting that during heavy smoke,
390 scattering and absorption of incoming PAR_g was enhanced.

391

392

393 **3.2 Biogeochemical responses**

394 **3.2.1 Net ecosystem exchange**

395 Daily totals for NEE are shown in Fig. 5. Both sites became a stronger CO_2 sink when
396 the smoke was present except in the September 2020 case. These increases were
397 statistically significant in the first two years. The average change in daily (24-h) totals
398 of NEE was about $-1.00 \text{ g C m}^{-2} \text{ day}^{-1}$ during the three years prior to 2020 with this
399 increase in sink strength primarily driven by an increase in GPP (Fig. 5). The increase
400 in GPP ($\sim 2.00 \text{ g C m}^{-2} \text{ day}^{-1}$) was more prominent than the decrease in R_e ($< 1.00 \text{ g C}$
401 $\text{m}^{-2} \text{ day}^{-1}$) in general. NEE during the September 2020 case did not change because
402 both GPP and R_e showed little response to the smoke.

403 Throughout the 2015 smoke period, Burns Bog remained a CO_2 sink and showed
404 an increasingly negative trend in NEE (stronger CO_2 sink) over the duration of the
405 smoke episode. Before the smoke arrived at the bog, the mean daily NEE was about $-$
406 $1.60 \text{ g C m}^{-2} \text{ day}^{-1}$. The peak biogeochemical impact of the smoke at Burns Bog
407 occurred on 7 July, which led to a daily NEE of $-3.64 \text{ g C m}^{-2} \text{ day}^{-1}$ (net CO_2 sink)
408 (Fig. S5). Conversely, on 5 July, when the peak reduction of K_d was observed, NEE
409 at the forest site became more positive (a greater atmospheric source of CO_2). The
410 Buckley Bay forest site became a strong net CO_2 sink on 6 and 7 July (-1.35 and $-$
411 $2.31 \text{ g C m}^{-2} \text{ day}^{-1}$, respectively) when the smoke had started to disperse (Fig. S6).

412 In 2017, Burns Bog again became a stronger CO_2 sink (daily NEE $< -2.5 \text{ g C m}^{-2}$
413 day^{-1}) for three days (4–6 August) due to smoke (Fig. S5). The biogeochemical
414 impacts of smoke were a little different at Buckley Bay, where daily NEE showed
415 little change until decreasing to $-5.40 \text{ g C m}^{-2} \text{ day}^{-1}$ (stronger CO_2 sink) on the last day
416 of the study period (Fig. S6).



417 During the 2018 episode, both sites became a CO₂ sink for three days that smoke
418 affected Burns Bog on later dates (13 to 15 August) compared to Buckley Bay (11 to
419 13 August) (Fig. S5 and S6). Both sites changed from being CO₂ neutral to being a
420 moderate CO₂ sink of about $-2.50 \text{ g C m}^{-2} \text{ day}^{-1}$.

421 Throughout the 2020 smoke period, when the diffuse fraction was the highest of
422 all cases (0.30 to 0.80) significant impacts on NEE were observed at both sites.
423 Buckley Bay and Burns Bog both became stronger CO₂ sinks between 11 and 12
424 September (going from -0.57 to $-4.00 \text{ g C m}^{-2} \text{ day}^{-1}$ and from -0.40 to -1.40 g C m^{-2}
425 day^{-1} , respectively) (Fig. S5 and S6). However, after PAR_g dropped to low values,
426 both sites turned into weak CO₂ sources (2.10 and $0.37 \text{ g C m}^{-2} \text{ day}^{-1}$ for Buckley Bay
427 and Burns Bog, respectively).

428
429

430 3.2.2 Gross primary production and ecosystem respiration

431 Measured NEE was partitioned into GPP and R_e to further investigate the
432 biogeochemical responses of the two sites to smoke (Fig. 5). In general, most of the
433 changes in GPP and R_e during the smoke periods compared to the non-smoky days
434 were statistically significant. In the 2015 smoke event at Buckley Bay, daily GPP
435 increased about 25% while daily R_e decreased by only about 5%, which resulted in the
436 site becoming a CO₂ sink. At Burns Bog, the responses were somewhat different than
437 those at Buckley Bay. Here, the relative increase in daily GPP and decrease in daily
438 R_e were similar with both being ~60%.

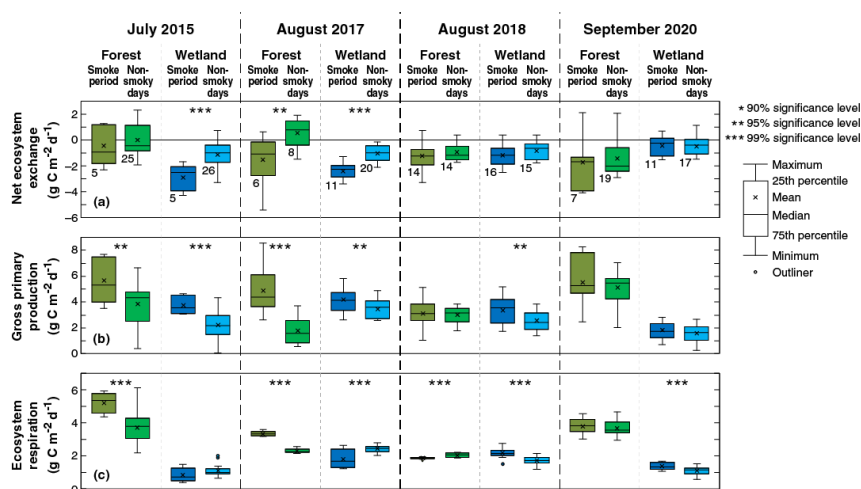
439 Due to missing data, the increase in CO₂ sequestration was only appreciable on
440 one day (6 August) at Buckley Bay in 2017 (Fig. S6). This was predominantly
441 controlled by the sizeable increase in daily GPP (140%), while the decrease in daily
442 R_e was minimal at 4%. The increase in daily GPP also played a role in increasing CO₂
443 sequestration at Burns Bog but it was not as strong as at Buckley Bay, where the
444 increases in daily GPP were about 30% and the decreases in daily R_e were smaller at
445 15%.

446 Compared to the previous two years where both sites became stronger CO₂ sinks
447 from being weak CO₂ sinks, the changes in 2018 at the two sites were similar but
448 slightly smaller. The main factor was the weaker rise in daily GPP. The Burns Bog
449 wetland site had about 30% higher daily GPP during the smoke event than during
450 non-smoky conditions (Fig. S5). But the Buckley Bay forest site experienced about
451 the same daily GPP during the smoke event as during non-smoky conditions (Fig.
452 S6).

453 Throughout the 2020 smoke event, there were marked increases in daily GPP of
454 about 90% at both sites. Due to the heavy smoke permitting only low PAR_g on 13



455 September, daily GPP rapidly dropped by about 70% compared to the previous days
 456 (Fig. S5 and S6). This resulted in the two sites switching from CO₂ sinks to sources
 457 over one day.
 458



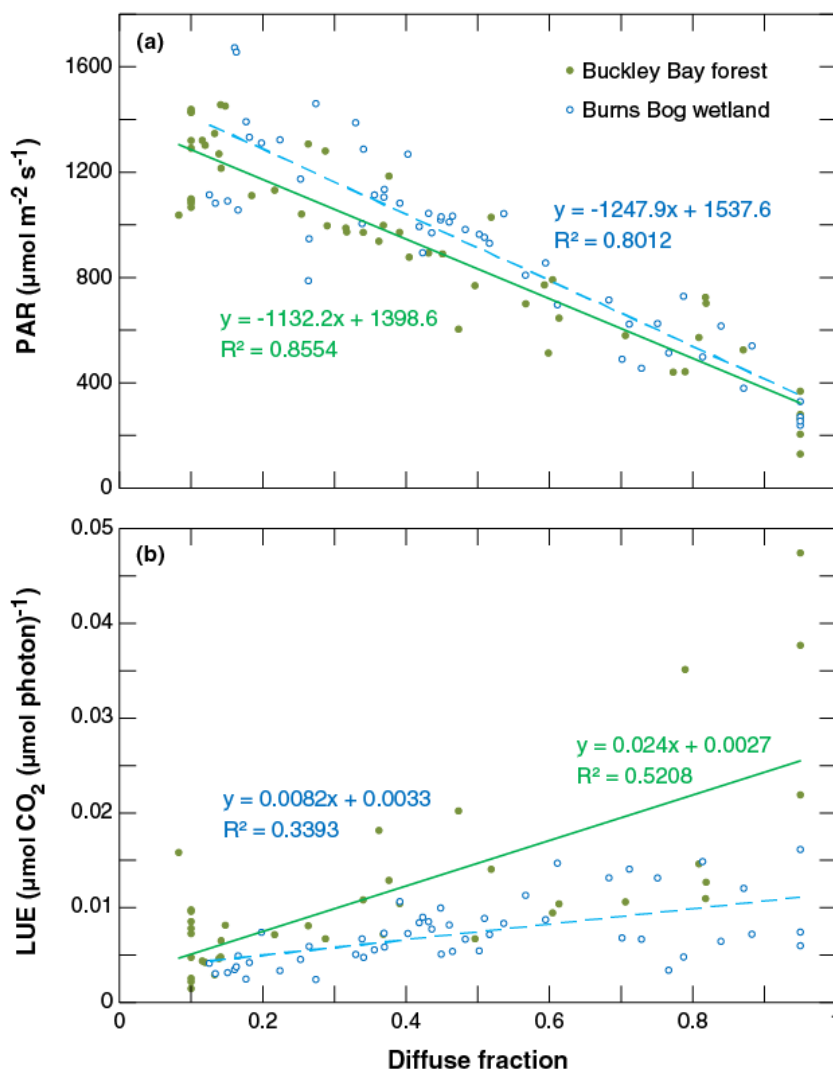
459
 460 **Figure 5.** Box plots of net ecosystem exchange (NEE), gross primary production
 461 (GPP), and ecosystem respiration (R_c) at the forest site during the smoke events and
 462 non-smoky days, respectively, in 2015, 2017, 2018, and 2020. The numbers of daily
 463 cases (n) used in the significance tests for each period for both the forest and wetland
 464 sites are shown beneath the boxplot pairs for the forest site in panel a. Unless
 465 otherwise shown, n is the same for all other variables and boxplot pairs in the same
 466 year.

467
 468

469 3.2.3 Relationship between smoke and gross primary production

470 Fig. 6a shows the dependence of mean PAR_g on the diffuse fraction for the two sites.
 471 As expected, PAR_g decreases linearly as the fraction increases ($R^2 = 0.86$ and 0.80 for
 472 Buckley Bay and Burns Bog, respectively). PAR_g decreased more rapidly ($\sim 10\%$) at
 473 the wetland site than the forest site. The relationship between LUE and the diffuse
 474 fraction was also examined in order to better understand the behaviour of the
 475 dependence of GPP on the diffuse fraction (Fig 6b). A linear relationship is evident
 476 with a R^2 at 0.52 and 0.34 for Buckley Bay and Burns Bog, respectively. LUE at the
 477 forest site increased much more when the diffuse fraction increased, which was ~ 2
 478 times more than at the wetland site.

479



480

481 **Figure 6.** (a) Total photosynthetically active radiation (PAR_g) as a function of the
482 diffuse fraction of PAR_g . (b) Light use efficiency (LUE) as a function of the diffuse
483 fraction of PAR_g .



484 4 Discussion

485 4.1 Impact of smoke episodes on radiation and biophysical properties

486 Over the four study years, significant perturbation of both the radiation and energy
487 budgets over the forest and wetland ecosystems in southwestern BC was observed
488 when a dense layer of wildfire smoke impacted the region. Generally, changes were
489 more pronounced at the Buckley Bay forest site on Vancouver Island.

490 The observed decreases in K_{\downarrow} at the two sites during the four study periods were
491 about 50% and 40% for the forest and wetland sites, respectively. These values are
492 comparable (Table 2) with reported reductions of total solar irradiance by forest fire
493 smoke in Brazil (the Brazilian Amazon with AOD₅₀₀ peaking at 3.0) and Africa
494 (Zambian savanna with AOD₅₀₀ peaking at 2.0) (Schafer et al., 2002). Similar
495 agreement is also apparent when compared with the 2010 fires in central Russia that
496 led to a reduction of K_{\downarrow} of about 40% (Chubarova et al., 2012) or 80 W m⁻² (Péré et
497 al., 2014) and the 2017 Chilean mega-fires that made K_{\downarrow} drop about 100 W m⁻²
498 (Lapere et al., 2021). The reduction of K_{\downarrow} from Rosário et al. (2013) was smaller at
499 about 55 W m⁻² when AOD₅₀₀ was near 2.0 during the 2002 biomass burning season in
500 south America. Although the AOD₅₅₀ value was slightly lower than this study,
501 Yamasoe et al. (2017) reported that K_{\downarrow} was reduced by about 50 W m⁻² over spring,
502 during the period of long range transport of biomass burning plumes, in São Paulo,
503 Brazil. In our study, we found that K_{\downarrow} dropped to near 0 W m⁻² and that lower values
504 were about 90% and 70% of non-smoky conditions at the forest and wetland sites,
505 respectively, in September 2020. The reduction was much greater than the previous
506 three smoke episodes.

507 As with K_{\downarrow} , turbulent heat fluxes (H and LE) were appreciably affected by
508 smoke at the two sites with a greater impact at the Buckley Bay forest site. These
509 results are consistent in both direction and magnitude with previous studies elsewhere
510 where the reduction in K_{\downarrow} due to aerosols in turn impacted H and LE (Feingold et al.,
511 2005; Jiang and Feingold, 2006; Mallet et al., 2009; Markowicz et al., 2021; Steiner et
512 al., 2013). It is important to note that these results were similar despite the cited
513 locations being in quite different geographical settings than in this study.
514 Furthermore, they were associated with significantly lower AOD₅₅₀ values than
515 observed in the four BC episodes.

516 It is important to note that energy partitioning can be very different in different
517 ecosystems (Steiner et al., 2013). As discussed above, H was reduced significantly at
518 the Buckley Bay forest site where canopy effects are most important. The possible
519 mechanism could be that the switch from high direct radiation to predominately
520 diffuse radiation during the smoke episodes likely caused the reduction in H as a
521 consequence of reduced heating of leaves in a highly coupled forest canopy



522 (Brümmer et al., 2012). In this study, the wetland site offers an interesting contrast to
523 the Buckley Bay forest site. As McKendry et al. (2019) noted, with standing water as
524 a result of restoration at the wetland site, and little physiological control on *LE*, the
525 impacts on the energy partitioning were modest compared to the physiologically
526 controlled *LE* at Buckley Bay. Another factor affecting energy partitioning is soil
527 moisture. Our results indicate that *LE* at the forest site dropped much more in 2017
528 and 2018 than 2015. This might be due to generally drier soil conditions in August
529 than in July, especially the extreme dry summer during which there was only 1 mm of
530 precipitation in July and August 2017 (Lee et al., 2020b). Soil moisture also plays a
531 role at the wetland site. Generally, the site also had higher *LE* than *H* during the
532 smoke episodes except in September 2020. This was likely because water level
533 dropped below the rooting depth of most bog vegetation (Lee et al., 2017). For both *H*
534 and *LE*, when the smoke arrived at the later stage of summer (September 2020),
535 impacts were the greatest of the four study periods. This was attributed to the fact that
536 both sites were dry after two months of low precipitation.

537 Only a slight increase in albedo was observed at both sites with the arrival of
538 smoke during the four study periods. This was probably due to reduction in specular
539 reflection during direct solar irradiance and an increase in diffuse reflection.
540 However, Nojarov et al. (2021) found that the albedo of the underlying surface greatly
541 affects the radiative effect of aerosols at Musala (altitude is 2925 m), Bulgaria. The
542 results indicated that aerosol amount, at surface level, has a negative radiative effect
543 when albedo values are low (< 0.4) but a positive radiative effect when albedo values
544 are high (> 0.4). They explained that higher albedo can lead to larger amounts of
545 reflected and scattered shortwave radiation, especially close to the earth's surface. At
546 higher aerosol amounts the result is an increase in the amount of scattered shortwave
547 radiation, which also increases the global solar radiation.



548 **Table 2.** Observed decreased shortwave irradiance (K_{\downarrow}) during the study smoke
 549 periods and several estimates from previously published studies.
 550

Event	AOD value	Decrease in K_{\downarrow}	Reference
2015, BC	AOD ₅₀₀ = ~4.5 AOD ₅₀₀ = ~3.0	52% or 180 W m ⁻² 30% or 104 W m ⁻²	Buckley Bay site Burns Bog site
2017, BC	AOD ₅₀₀ = ~1.5 AOD ₅₀₀ = ~2.5	31% or 101 W m ⁻² 37% or 98 W m ⁻²	Buckley Bay site Burns Bog site
2018, BC	AOD ₅₀₀ = ~3.5	50% or 157 W m ⁻² 47% or 120 W m ⁻²	Buckley Bay site Burns Bog site
2020, BC	AOD ₅₀₀ not available	87% or 231 W m ⁻² 69% or 120 W m ⁻²	Buckley Bay site Burns Bog site
1999, Brazil	AOD ₅₀₀ = 0.5~3.0	9~37%	Schafer et al. (2002)
2000, Africa	AOD ₅₀₀ = 0.5~2.0	13~37%	Schafer et al. (2002)
2010, central Russia	AOD ₅₀₀ = 2.5	40%	Chubarova et al. (2012)
2002, South America	AOD ₅₀₀ = 0.2~2.0	10~55 W m ⁻²	Rosário et al. (2013)
2010, Central Russia	AOD ₃₄₀ = 2.0~4.0	70~84 W m ⁻²	Péré et al. (2014)
2005~2015, Brazil	AOD ₅₅₀ = 0.6~1.0	50 W m ⁻²	Yamasoe et al. (2017)
2017, Chile	AOD ₅₅₀ = 4.0	100 W m ⁻²	Lapere et al. (2021)

551



552 **4.2 Effects of aerosol loading on biogeochemical properties**

553 The typical diffuse fraction in southwestern BC under sunny conditions ($T > 0.65$)
554 over these four years was ~ 0.15 . Generally, when the diffuse fraction increased to
555 between 0.40 and 0.50 due to wildfire smoke, the two sites became a strong CO_2 sink
556 (i.e., NEE became more negative). However, these responses were also controlled by
557 other factors, such as VPD and T_s . When PAR_g dropped to low values, even if PAR_d
558 fraction exceeded 0.80, the study forest and wetland ecosystems both became a CO_2
559 source. These broad patterns are comparable to previous research in different
560 environments (Niyogi et al., 2004; Park et al., 2018; Yamasoe et al., 2006). An
561 observational study in the Amazon rainforest found that, under moderate AOD_{500} ,
562 CO_2 uptake was enhanced by the increased diffuse fraction (Yamasoe et al., 2006).
563 Park et al. (2018) also indicated that moderate levels of smoke resulted in small
564 increases in CO_2 sequestration, while extremely smoky conditions resulted in lower
565 CO_2 sequestration as the effect of the reduction in PAR_g outweighed the DRF effect.

566 The changes in NEE were primarily controlled by GPP (Fig. 5). Therefore, in
567 this study, we further investigated how GPP responded to smoke using the
568 relationship between PAR_g and diffuse fraction, as well as the relationship between
569 LUE and diffuse fraction. Ezhova et al. (2018) analyzed data from five forest sites
570 that included two mixed forests and three Scots pine (*Pinus sylvestris* L.) forests (55-,
571 60-, and 100-year old). In that region, diffuse fraction was approximately 0.11 on
572 days characterized by low aerosol loading and about 0.25 on days with moderate
573 aerosol loading. They also found that PAR_g decreased as diffuse fraction increased at
574 the five sites. Compared to their estimated coefficients (PAR_g at zero diffuse fraction),
575 the Buckley Bay forest site had a similar value ($-1132 \mu\text{mol m}^{-2} \text{s}^{-1}$) to the 100-year
576 old Scots pine forest ($-1118 \mu\text{mol m}^{-2} \text{s}^{-1}$). The Burns Bog wetland site had a slightly
577 higher coefficient ($-1248 \mu\text{mol m}^{-2} \text{s}^{-1}$) among all these sites ($-944 \mu\text{mol m}^{-2} \text{s}^{-1}$ to
578 about $-1194 \mu\text{mol m}^{-2} \text{s}^{-1}$). Generally, the slopes of the linear dependences in the
579 relationship of PAR_g and diffuse fraction were similar, which can likely be attributed
580 to similar cloud attenuating properties (Ezhova et al., 2018).

581 The slope in the relationship of LUE and diffuse fraction reflects canopy
582 properties. The Buckley Bay forest site had a slope of $0.0240 \mu\text{mol CO}_2 (\mu\text{mol}$
583 $\text{photon})^{-1}$, which is about three times higher than the value found at the Burns Bog
584 wetland site ($0.0082 \mu\text{mol CO}_2 (\mu\text{mol photon})^{-1}$). This indicates the ability of a forest
585 stand to take up more CO_2 in response to an increasing diffuse fraction of PAR.
586 Ezhova et al. (2018) found that two mixed forest sites (0.0238 to $0.0278 \mu\text{mol CO}_2$
587 $(\mu\text{mol photon})^{-1}$) had steeper LUE slopes compared to the other three coniferous
588 forest sites (about $0.015 \mu\text{mol CO}_2 (\mu\text{mol photon})^{-1}$ in average). They attributed the
589 difference to mixed forests having a larger potential for photosynthetic activity



590 enhancement due to a larger leaf area index and a deeper canopy. Results from mixed
591 and broadleaf forest sites in the USA showed the increase in LUE was about 0.03
592 $\mu\text{mol CO}_2 (\mu\text{mol photon})^{-1}$ (Cheng et al., 2016). Hemes et al. (2020) analyzed the EC
593 measurements across one corn (C4 plant), one alfalfa (C3 plant), and two restored
594 wetland (C3 plants) sites during the summer 2018 smoke event in California, USA.
595 The slope of the relationship between LUE and diffuse fraction for the corn site
596 ($0.0190 \mu\text{mol CO}_2 (\mu\text{mol photon})^{-1}$) was intermediate between the mature alfalfa site
597 ($0.0270 \mu\text{mol CO}_2 (\mu\text{mol photon})^{-1}$) and the two restored wetland sites (0.0140 and
598 $0.0180 \mu\text{mol CO}_2 (\mu\text{mol photon})^{-1}$). This indicates that corn is more sensitive than the
599 wetlands but less than alfalfa. Their restored wetland ecosystems are both
600 characterized by quasi-managed mixes of tule and cattail vegetation with
601 aboveground water tables. Thus, these two sites had lower LUE sensitivities to diffuse
602 fraction compared to the two crop sites. Our wetland site has even shorter vegetation
603 compared to theirs and thus an even lower sensitivity ($\sim 40\%$ lower).

604 Finally, based on the linear dependence of LUE on diffuse fraction and PAR_g on
605 diffuse fraction, we estimated how GPP changed with diffuse fraction. GPP at the
606 Buckley Bay forest site can increase up to $\sim 18\%$, which is consistent with results
607 from Ezhova et al. (2018) showing an increase in GPP between 6% and 14% at five
608 forest sites. Hemes et al. (2020) found that the GPP enhancement was between 0.71%,
609 and 1.16% at four sites for every 1% increase in diffuse fraction when absorbed PAR_g
610 was held constant. Lee et al. (2018) also showed a comparable GPP enhancement at
611 0.94% GPP using a process-based sun-shade canopy model with observations from a
612 broadleaf forest in the eastern USA. We note that although the empirical models
613 based on conditional sampling in this study are able to explain much of the variation
614 in observations, they have limitations compared to more mechanistic, process-based
615 models (Knobl and Baldocchi, 2008; Lee et al., 2018). On the other hand, process-
616 based models often require parameterizations for specific vegetation and
617 photosynthetic types that introduce more complexities and hence probably lead to
618 higher uncertainty (Hemes et al., 2020).

619

620 **4.3 Study limitations**

621 Due to their limited spatial and temporal scale, the results described here have
622 limitations that restrict attempts to generalise (and easily scale up). Firstly, although
623 the four cases examined extend our understanding of biophysical and biogeochemical
624 impacts to a wider range of cases than McKendry et al. (2020), they are by no means
625 exhaustive, nor are they likely representative of the broad variety of forest types
626 across BC.



627 Secondly, attribution of ecosystem responses wholly to smoke, while rigorously
628 controlling for other environmental variables (e.g. air quality, antecedent moisture
629 conditions, wind, cloudiness, RH, temperature) is challenging. Our rudimentary tests
630 of significance highlight that whilst there is a clear signal of biophysical and
631 biogeochemical responses to smoke, it is by no means consistent across all four
632 events, each land-use type, or all variables. This suggests that each smoke event is
633 somewhat unique in terms of antecedent conditions, present weather conditions and
634 the characteristics of the smoke itself (e.g. age, elevation, composition, density). For
635 example, in addition to the effects of diffuse fraction, wildfire smoke often
636 incorporates a complex mixture of gases (e.g., CO, CH₄, NO_x, and O₃), aerosols, and
637 aerosol precursors (Crutzen et al., 1979; Jaffe and Wigder, 2012; Pfister et al., 2008).
638 Increased O₃ and co-pollutants are often associated with wildfires (Jaffe & Wigder,
639 2012; Pfister et al., 2008; Yamasoe et al., 2006) and can have an indirect impact on
640 the ecosystem carbon budget that is harder to quantify (Malavelle et al., 2019). None
641 of these effects are addressed in this study.

642 Finally, we have compared smoky and non-smoky conditions exclusively during
643 the months of these events. This is somewhat arbitrary and necessarily neglects a wide
644 range of meteorological variability associated with each “type”. However, this
645 rudimentary approach serves to highlight the complex combination of processes
646 involved. Various combinations of cloudiness, antecedent meteorological conditions,
647 wind, etc. all control biophysical and biogeochemical responses, with smoke being
648 only one of the factors at play. Isolating the individual impact of smoke is
649 challenging. There are, however, common elements that can be gleaned from this
650 inter-comparison of four cases. In particular, the presence of wildfire smoke is shown
651 to have a statistically significant impact on diffuse radiation that has the potential to
652 turn both natural and managed ecosystems into a carbon sink when smoke densities
653 are low to moderate. In this sense, this work is consistent with both theory and
654 observations elsewhere and confirms that wildfire smoke likely has a significant
655 impact on regional carbon budgets.



656 **5 Conclusions**

657 Aerosol loading from wildfire smoke is not only becoming a regular component of air
658 quality considerations in a warming world but has climate impacts and unexplored
659 feedbacks. Through biogeochemical and biophysical processes, wildfire smoke
660 influences the climate by altering both greenhouse gas dynamics and how energy and
661 water are exchanged between the ecosystem and the atmosphere. Clearly, under
662 conditions in which the presence of wildfire smoke is more frequent, and perhaps of
663 longer duration, the results described herein imply substantial impacts on the regional
664 carbon budget.

665

666 Results from four major smoke events in different years are broadly consistent with
667 those described elsewhere. Specifically for the two sites examined;

- 668 • The reduction in incoming solar radiation due to smoke was generally about
669 50% but reached 90% in the September 2020 case and was near 100% in dense
670 smoke.
- 671 • The forest site had a more dramatic change in the ratio of sensible heat to latent
672 heat flux (i.e., the Bowen ratio). When the smoke arrived later (e.g., September
673 2020), impacts on turbulent heat fluxes were the greatest for both sites. This was
674 attributed to the markedly reduced incoming solar radiation and to both sites
675 being dry after two months of low precipitation.
- 676 • Under non-smoky conditions during the summer months, diffuse fraction in
677 southwestern British Columbia is ~ 0.30 . The presence of smoke generally
678 increased it to ~ 0.50 with dense smoke increasing values to ~ 0.95 . When total
679 photosynthetically active radiation dropped to low values, however, both the
680 forest and wetland ecosystems turned into CO_2 sources.
- 681 • Photosynthesis can be increased by $\sim 18\%$ and $\sim 7\%$ due to the direct effect of
682 smoke particles compared to clean conditions in the forest and wetland sites,
683 respectively.

684

685 This study confirms a clear signal of diffuse radiation fertilization across four major
686 smoke episodes, resulting in forest and wetland becoming enhanced carbon sinks
687 under some smoke conditions. This has implications for the regional carbon budget if
688 the duration and frequency of smoke events increases as a result of climate change.
689 However, we identify significant limitations in this preliminary research and identify
690 a complex array of processes that contribute to biophysical and biogeochemical
691 responses. Before attempting to scale up, further research is required in different
692 forest types across the region and to identify and control for the myriad processes and
693 feedbacks influencing local carbon budgets in forest and wetland ecosystems.



694 **6 Acknowledgements**

695 We are grateful to the Natural Sciences and Engineering Research Council of Canada
696 (NSERC) for support to individual researchers and graduate students involved in this
697 work. The Buckley Bay flux tower was funded by the NSERC and The Canadian
698 Foundation for Innovation (CFI). We sincerely thank Island Timberlands LP for the
699 permission to work on their land and their logistical support. The Burns Bog flux
700 tower operation was funded by Metro Vancouver through contracts to Drs. Andreas
701 Christen and Sara Knox. Selected instrumentation was supported by NSERC and CFI.
702 We thanks the substantial technical and logistical support by staffs from Metro
703 Vancouver and City of Delta. We greatly appreciate the assistance of Robert Halsall,
704 Rick Ketler, Zoran Nestic, and Marion Nyberg with the invaluable field and technical
705 support.



706 **7 References**

- 707 Alton, P., Mercado, L. and North, P.: A sensitivity analysis of the land-surface scheme
708 JULES conducted for three forest biomes: Biophysical parameters, model processes,
709 and meteorological driving data, *Global Biogeochem. Cycles*, 20(1), 2006.
- 710 Alton, P. B.: Reduced carbon sequestration in terrestrial ecosystems under overcast
711 skies compared to clear skies, *Agric. For. Meteorol.*, 148(10), 1641–1653, 2008.
- 712 Barr, A. G., Black, T. A., Hogg, E. H., Kljun, N., Morgenstern, K. and Nesic, Z.: Inter-
713 annual variability in the leaf area index of a boreal aspen-hazelnut forest in relation to
714 net ecosystem production, *Agric. For. Meteorol.*, 126(3–4), 237–255, 2004.
- 715 Black, T. A.: AmeriFlux BASE CA-Ca3 British Columbia - Pole sapling Douglas-fir
716 stand, Ver. 3-5, AmeriFlux AMP, (Dataset). <https://doi.org/10.17190/AMF/1480302>,
717 2021.
- 718 Brümmer, C., Black, T. A., Jassal, R. S., Grant, N. J., Spittlehouse, D. L., Chen, B.,
719 Nesic, Z., Amiro, B. D., Arain, M. A. and Barr, A. G.: How climate and vegetation
720 type influence evapotranspiration and water use efficiency in Canadian forest,
721 peatland and grassland ecosystems, *Agric. For. Meteorol.*, 153, 14–30, 2012.
- 722 Chen, B., Black, T. A., Coops, N. C., Hilker, T., Trofymow, J. A. T. and Morgenstern,
723 K.: Assessing tower flux footprint climatology and scaling between remotely sensed
724 and eddy covariance measurements, *Boundary-Layer Meteorol.*, 130(2), 137–167,
725 2009.
- 726 Cheng, S. J., Bohrer, G., Steiner, A. L., Hollinger, D. Y., Suyker, A., Phillips, R. P.
727 and Nadelhoffer, K. J.: Variations in the influence of diffuse light on gross primary
728 productivity in temperate ecosystems, *Agric. For. Meteorol.*, 201, 98–110, 2015.
- 729 Cheng, S. J., Steiner, A. L., Hollinger, D. Y., Bohrer, G. and Nadelhoffer, K. J.: Using
730 satellite-derived optical thickness to assess the influence of clouds on terrestrial
731 carbon uptake, *J. Geophys. Res. Biogeosciences*, 121(7), 1747–1761, 2016.
- 732 Christen, A., Jassal, R. S., Black, T. A., Grant, N. J., Hawthorne, I., Johnson, M. S.,
733 Lee, S.-C. and Merckens, M.: Summertime greenhouse gas fluxes from an urban bog
734 undergoing restoration through rewetting., *Mires Peat*, 17, 2016.
- 735 Christen, A., and Knox, S.: AmeriFlux BASE CA-DBB Delta Burns Bog, Ver. 2-5,
736 AmeriFlux AMP, (Dataset). <https://doi.org/10.17190/AMF/1543378>, 2021
- 737 Chubarova, N., Nezval, Y., Sviridenkov, I., Smirnov, A. and Slutsker, I.: Smoke
738 aerosol and its radiative effects during extreme fire event over Central Russia in
739 summer 2010, *Atmos. Meas. Tech.*, 5(3), 557, 2012.
- 740 Crutzen, P. J. and Andreae, M. O.: Biomass burning in the tropics: Impact on
741 atmospheric chemistry and biogeochemical cycles, *Science* (80-.), 250(4988), 1669–
742 1678, 1990.



- 743 Crutzen, P. J., Heidt, L. E., Krasnec, J. P., Pollock, W. H. and Seiler, W.: Biomass
744 burning as a source of atmospheric gases CO, H₂, N₂O, NO, CH₃Cl and COS, *Nature*,
745 282(5736), 253–256, 1979.
- 746 D’Acunha, B., Morillas, L., Black, T. A., Christen, A. and Johnson, M. S.: Net
747 ecosystem carbon balance of a peat bog undergoing restoration: integrating CO₂ and
748 CH₄ fluxes from eddy covariance and aquatic evasion with DOC drainage fluxes, *J.*
749 *Geophys. Res. Biogeosciences*, 124(4), 884–901, 2019.
- 750 Doughty, C. E., Flanner, M. G. and Goulden, M. L.: Effect of smoke on subcanopy
751 shaded light, canopy temperature, and carbon dioxide uptake in an Amazon rainforest,
752 *Global Biogeochem. Cycles*, 24(3), 2010.
- 753 Ezhova, E., Ylivinkka, I., Kuusk, J., Komsaare, K., Vana, M., Krasnova, A., Noe, S.,
754 Arshinov, M., Belan, B. and Park, S.-B.: Direct effect of aerosols on solar radiation
755 and gross primary production in boreal and hemiboreal forests, *Atmos. Chem. Phys.*,
756 2018.
- 757 Feingold, G., Jiang, H. and Harrington, J. Y.: On smoke suppression of clouds in
758 Amazonia, *Geophys. Res. Lett.*, 32(2), 2005.
- 759 Ferrara, M., Pomeroy, C., McKendry, I. G., Stull, R. and Strawbridge, K.: Suppression
760 of “Handover” Processes in a Mountain Convective Boundary Layer due to Persistent
761 Wildfire Smoke, *Boundary-Layer Meteorol.*, 1–12, 2020.
- 762 Gu, L., Baldocchi, D., Verma, S. B., Black, T. A., Vesala, T., Falge, E. M. and Dowty,
763 P. R.: Advantages of diffuse radiation for terrestrial ecosystem productivity, *J.*
764 *Geophys. Res. Atmos.*, 107(D6), ACL-2, 2002.
- 765 Hemes, K. S., Verfaillie, J. and Baldocchi, D. D.: Wildfire-smoke aerosols lead to
766 increased light use efficiency among agricultural and restored wetland land uses in
767 California’s Central Valley, *J. Geophys. Res. Biogeosciences*, 125(2),
768 e2019JG005380, 2020.
- 769 Hollinger, D. Y., Kelliher, F. M., Byers, J. N., Hunt, J. E., McSeveny, T. M. and Weir,
770 P. L.: Carbon dioxide exchange between an undisturbed old-growth temperate forest
771 and the atmosphere, *Ecology*, 75(1), 134–150, 1994.
- 772 Hovi, A., Liang, J., Korhonen, L., Kobayashi, H. and Rautiainen, M.: Quantifying the
773 missing link between forest albedo and productivity in the boreal zone,
774 *Biogeosciences*, 13(21), 6015–6030, 2016.
- 775 Humphreys, E. R., Black, T. A., Morgenstern, K., Cai, T., Drewitt, G. B., Nestic, Z.
776 and Trofymow, J. A.: Carbon dioxide fluxes in coastal Douglas-fir stands at different
777 stages of development after clearcut harvesting, *Agric. For. Meteorol.*, 140(1–4), 6–
778 22, 2006.



- 779 Jacobson, M. Z.: Effects of biomass burning on climate, accounting for heat and
780 moisture fluxes, black and brown carbon, and cloud absorption effects, *J. Geophys.*
781 *Res. Atmos.*, 119(14), 8980–9002, 2014.
- 782 Jaffe, D. A. andWigder, N. L.: Ozone production from wildfires: A critical review,
783 *Atmos. Environ.*, 51, 1–10, 2012.
- 784 Jassal, R. S., Black, T. A., Spittlehouse, D. L., Brümmer, C. andNesic, Z.:
785 Evapotranspiration and water use efficiency in different-aged Pacific Northwest
786 Douglas-fir stands, *Agric. For. Meteorol.*, 149(6–7), 1168–1178, 2009.
- 787 Jiang, H. andFeingold, G.: Effect of aerosol on warm convective clouds: Aerosol-
788 cloud-surface flux feedbacks in a new coupled large eddy model, *J. Geophys. Res.*
789 *Atmos.*, 111(D1), 2006.
- 790 Kanniah, K. D., Beringer, J., North, P. andHutley, L.: Control of atmospheric particles
791 on diffuse radiation and terrestrial plant productivity: A review, *Prog. Phys. Geogr.*,
792 36(2), 209–237, 2012.
- 793 Knohl, A. andBaldocchi, D. D.: Effects of diffuse radiation on canopy gas exchange
794 processes in a forest ecosystem, *J. Geophys. Res. Biogeosciences*, 113(G2), 2008.
- 795 Krishnan, P., Black, T. A., Jassal, R. S., Chen, B. andNesic, Z.: Interannual variability
796 of the carbon balance of three different-aged Douglas-fir stands in the Pacific
797 Northwest, *J. Geophys. Res. Biogeosciences*, 114(G4), 2009.
- 798 Landry, J.-S., Matthews, H. D. andRamankutty, N.: A global assessment of the carbon
799 cycle and temperature responses to major changes in future fire regime, *Clim.*
800 *Change*, 133(2), 179–192, 2015.
- 801 Lapere, R., Mailler, S. andMenut, L.: The 2017 Mega-Fires in Central Chile: Impacts
802 on Regional Atmospheric Composition and Meteorology Assessed from Satellite Data
803 and Chemistry-Transport Modeling, *Atmosphere (Basel)*, 12(3), 344, 2021.
- 804 Lasslop, G., Coppola, A. I., Voulgarakis, A., Yue, C. andVeraverbeke, S.: Influence
805 of fire on the carbon cycle and climate, *Curr. Clim. Chang. Reports*, 5(2), 112–123,
806 2019.
- 807 Lee, M. S., Hollinger, D. Y., Keenan, T. F., Ouimette, A. P., Ollinger, S.V
808 andRichardson, A. D.: Model-based analysis of the impact of diffuse radiation on
809 CO₂ exchange in a temperate deciduous forest, *Agric. For. Meteorol.*, 249, 377–389,
810 2018.
- 811 Lee, S.-C., Black, T. A., Jassal, R. S., Christen, A., Meyer, G. andNesic, Z.: Long-
812 term impact of nitrogen fertilization on carbon and water fluxes in a Douglas-fir stand
813 in the Pacific Northwest, *For. Ecol. Manage.*, 455, 117645, 2020a.
- 814 Lee, S.-C., Christen, A., Black, T. A., Jassal, R. S., Ketler, R. andNesic, Z.:
815 Partitioning of net ecosystem exchange into photosynthesis and respiration using



816 continuous stable isotope measurements in a Pacific Northwest Douglas-fir forest
817 ecosystem, *Agric. For. Meteorol.*, 292, 108109, 2020b.

818 Lee, S. C., Christen, A., Black, A. T., Johnson, M. S., Jassal, R. S., Ketler, R., Nestic,
819 Z. and Merckens, M.: Annual greenhouse gas budget for a bog ecosystem undergoing
820 restoration by rewetting, *Biogeosciences*, 14(11), 2799–2814, 2017.

821 Letts, M. G., Lafleur, P. M. and Roulet, N. T.: On the relationship between cloudiness
822 and net ecosystem carbon dioxide exchange in a peatland ecosystem, *Ecoscience*,
823 12(1), 53–69, 2005.

824 Malavelle, F. F., Haywood, J. M., Mercado, L. M., Folberth, G. A., Bellouin, N.,
825 Sitch, S. and Artaxo, P.: Studying the impact of biomass burning aerosol radiative and
826 climate effects on the Amazon rainforest productivity with an Earth system model,
827 *Atmos. Chem. Phys.*, 19(2), 1301–1326, 2019.

828 Mallet, M., Tulet, P., Serça, D., Solmon, F., Dubovik, O., Pelon, J., Pont, V.
829 and Thouron, O.: Impact of dust aerosols on the radiative budget, surface heat fluxes,
830 heating rate profiles and convective activity over West Africa during March 2006,
831 *Atmos. Chem. Phys.*, 9(18), 7143–7160, 2009.

832 Markowicz, K. M., Lisok, J. and Xian, P.: Simulations of the effect of intensive
833 biomass burning in July 2015 on Arctic radiative budget, *Atmos. Environ.*, 171, 248–
834 260, 2017.

835 Markowicz, K. M., Zawadzka-Manko, O., Lisok, J., Chilinski, M. T. and Xian, P.: The
836 impact of moderately absorbing aerosol on surface sensible, latent, and net radiative
837 fluxes during the summer of 2015 in Central Europe, *J. Aerosol Sci.*, 151, 105627,
838 2021.

839 McKendry, I., Strawbridge, K., Karumudi, M. L., O’Neill, N., Macdonald, A. M.,
840 Leitch, R., Jaffe, D., Cottle, P., Sharma, S. and Sheridan, P.: Californian forest fire
841 plumes over Southwestern British Columbia: lidar, sunphotometry, and mountaintop
842 chemistry observations, *Atmos. Chem. Phys.*, 11(2), 465–477, 2011.

843 McKendry, I. G., Christen, A., Sung-Ching, L., Ferrara, M., Strawbridge, K. B.,
844 O’Neill, N. and Black, A.: Impacts of an intense wildfire smoke episode on surface
845 radiation, energy and carbon fluxes in southwestern British Columbia, Canada,
846 *Atmos. Chem. Phys.*, 19(2), 835–846, 2019.

847 Millennium Ecosystem Assessment: Ecosystems and human well-being, Island press
848 United States of America., 2005.

849 Ministry of Forests: British Columbia’s forests: and their management. [online]
850 Available from: <https://www.for.gov.bc.ca/hfd/pubs/Docs/Mr/Mr113.htm>, 2003.

851 Ministry of Forests Mines and Land: The State of British Columbia’s Forests Th_ird
852 Edition. [online] Available from:



- 853 [https://www2.gov.bc.ca/assets/gov/environment/research-monitoring-and-](https://www2.gov.bc.ca/assets/gov/environment/research-monitoring-and-reporting/reporting/envreportbc/archived-reports/sof_2010.pdf)
854 [reporting/reporting/envreportbc/archived-reports/sof_2010.pdf](https://www2.gov.bc.ca/assets/gov/environment/research-monitoring-and-reporting/reporting/envreportbc/archived-reports/sof_2010.pdf), 2010.
- 855 Moncrieff, J. B., Massheder, J. M., DeBruin, H., Elbers, J., Friborg, T., Heusinkveld,
856 B., Kabat, P., Scott, S., Sørensen, H. and Verhoef, A.: A system to measure surface
857 fluxes of momentum, sensible heat, water vapour and carbon dioxide, *J. Hydrol.*, 188,
858 589–611, 1997.
- 859 Moreira, D. S., Longo, K. M., Freitas, S. R., Yamasoe, M. A., Mercado, L. M.,
860 Rosário, N. E., Gloor, E., Viana, R. S. M., Miller, J. B. and Gatti, L. V.: Modeling the
861 radiative effects of biomass burning aerosols on carbon fluxes in the Amazon region,
862 2017.
- 863 Morgenstern, K., Black, T. A., Humphreys, E. R., Griffis, T. J., Drewitt, G. B., Cai,
864 T., Nesic, Z., Spittlehouse, D. L. and Livingston, N. J.: Sensitivity and uncertainty of
865 the carbon balance of a Pacific Northwest Douglas-fir forest during an El Niño/La
866 Niña cycle, *Agric. For. Meteorol.*, 123(3–4), 201–219, 2004.
- 867 Niyogi, D., Chang, H., Saxena, V. K., Holt, T., Alapaty, K., Booker, F., Chen, F.,
868 Davis, K. J., Holben, B. and Matsui, T.: Direct observations of the effects of aerosol
869 loading on net ecosystem CO₂ exchanges over different landscapes, *Geophys. Res.*
870 *Lett.*, 31(20), 2004.
- 871 Nojarov, P., Arsov, T., Kalapov, I. and Angelov, H.: Aerosol direct effects on global
872 solar shortwave irradiance at high mountainous station Musala, Bulgaria, *Atmos.*
873 *Environ.*, 244, 117944, 2021.
- 874 Oliphant, A. J., Dragoni, D., Deng, B., Grimmond, C. S. B., Schmid, H.-P. and Scott,
875 S. L.: The role of sky conditions on gross primary production in a mixed deciduous
876 forest, *Agric. For. Meteorol.*, 151(7), 781–791, 2011.
- 877 Oris, F., Asselin, H., Ali, A. A., Finsinger, W. and Bergeron, Y.: Effect of increased
878 fire activity on global warming in the boreal forest, *Environ. Rev.*, 22(3), 206–219,
879 2014.
- 880 Pachauri, R. K., Allen, M. R., Barros, V. R., Broome, J., Cramer, W., Christ, R.,
881 Church, J. A., Clarke, L., Dahe, Q. and Dasgupta, P.: Climate change 2014: synthesis
882 report. Contribution of Working Groups I, II and III to the fifth assessment report of
883 the Intergovernmental Panel on Climate Change, *Ippc.*, 2014.
- 884 Papale, D., Reichstein, M., Aubinet, M., Canfora, E., Bernhofer, C., Kutsch, W.,
885 Longdoz, B., Rambal, S., Valentini, R. and Vesala, T.: Towards a standardized
886 processing of Net Ecosystem Exchange measured with eddy covariance technique:
887 algorithms and uncertainty estimation, *Biogeosciences*, 3(4), 571–583, 2006.
- 888 Park, S.-B., Knohl, A., Lucas-Moffat, A. M., Migliavacca, M., Gerbig, C., Vesala, T.,
889 Peltola, O., Mammarella, I., Kolle, O. and Lavrič, J. V.: Strong radiative effect



890 induced by clouds and smoke on forest net ecosystem productivity in central Siberia,
891 *Agric. For. Meteorol.*, 250, 376–387, 2018.

892 Péré, J. C., Bessagnet, B., Mallet, M., Waquet, F., Chiapello, I., Minvielle, F., Pont,
893 V. and Menut, L.: Direct radiative effect of the Russian wildfires and its impact on air
894 temperature and atmospheric dynamics during August 2010, *Atmos. Chem. Phys.*,
895 14(4), 1999–2013, 2014.

896 Pfister, G. G., Wiedinmyer, C. and Emmons, L. K.: Impacts of the fall 2007 California
897 wildfires on surface ozone: Integrating local observations with global model
898 simulations, *Geophys. Res. Lett.*, 35(19), 2008.

899 R Core Team: R: A language and environment for statistical computing, [online]
900 Available from: <https://www.r-project.org/>, 2017.

901 Rap, A., Spracklen, D. V., Mercado, L., Reddington, C. L., Haywood, J. M., Ellis, R.
902 J., Phillips, O. L., Artaxo, P., Bonal, D. and Restrepo Coupe, N.: Fires increase
903 Amazon forest productivity through increases in diffuse radiation, *Geophys. Res.*
904 *Lett.*, 42(11), 4654–4662, 2015.

905 Reichstein, M., Falge, E., Baldocchi, D., Papale, D., Aubinet, M., Berbigier, P.,
906 Bernhofer, C., Buchmann, N., Gilmanov, T. and Granier, A.: On the separation of net
907 ecosystem exchange into assimilation and ecosystem respiration: review and
908 improved algorithm, *Glob. Chang. Biol.*, 11(9), 1424–1439, 2005.

909 Rosário, N. E. do, Longo, K. M., Freitas, S. R. de, Yamasoe, M. A. and Fonseca, R.
910 M. da: Modeling the South American regional smoke plume: aerosol optical depth
911 variability and surface shortwave flux perturbation, *Atmos. Chem. Phys.*, 13(6),
912 2923–2938, 2013.

913 Schafer, J. S., Eck, T. F., Holben, B. N., Artaxo, P., Yamasoe, M. A. and Procopio, A.
914 S.: Observed reductions of total solar irradiance by biomass-burning aerosols in the
915 Brazilian Amazon and Zambian Savanna, *Geophys. Res. Lett.*, 29(17), 1–4, 2002.

916 Sena, E. T., Artaxo, P. and Correia, A. L.: Spatial variability of the direct radiative
917 forcing of biomass burning aerosols and the effects of land use change in Amazonia.,
918 *Atmos. Chem. Phys.*, 13(3), 2013.

919 Settele, J., Scholes, R., Betts, R. A., Bunn, S., Leadley, P., Nepstad, D., Overpeck, J.,
920 Taboada, M. A., Fischlin, A. and Moreno, J. M.: Terrestrial and inland water systems,
921 in *Climate change 2014 impacts, adaptation and vulnerability: Part A: Global and*
922 *sectoral aspects*, pp. 271–360, Cambridge University Press., 2015.

923 Steiner, A. L., Mermelstein, D., Cheng, S. J., Twine, T. E. and Oliphant, A.: Observed
924 impact of atmospheric aerosols on the surface energy budget, *Earth Interact.*, 17(14),
925 1–22, 2013.

926 Strada, S., Unger, N. and Yue, X.: Observed aerosol-induced radiative effect on plant
927 productivity in the eastern United States, *Atmos. Environ.*, 122, 463–476, 2015.



928 Taubman, B. F., Marufu, L. T., Vant-Hull, B. L., Piety, C. A., Doddridge, B. G.,
929 Dickerson, R. R. and Li, Z.: Smoke over haze: Aircraft observations of chemical and
930 optical properties and the effects on heating rates and stability, *J. Geophys. Res.*
931 *Atmos.*, 109(D2), 2004.

932 Ward, D. S., Kloster, S., Mahowald, N. M., Rogers, B. M., Randerson, J. T. and Hess,
933 P. G.: The changing radiative forcing of fires: global model estimates for past, present
934 and future, *Atmos. Chem. Phys.*, 12(22), 10857–10886, 2012.

935 Wetland Stewardship Partnership: Wetland Ways: Interim Guidelines for Wetland
936 Protection and Conservation in British Columbia. [online] Available from:
937 [https://www2.gov.bc.ca/gov/content/environment/air-land-water/water/water-](https://www2.gov.bc.ca/gov/content/environment/air-land-water/water/water-planning-strategies/wetlands-in-bc#:~:text=British Columbia%27s wetlands currently)
938 [planning-strategies/wetlands-in-bc#:~:text=British Columbia%27s wetlands currently](https://www2.gov.bc.ca/gov/content/environment/air-land-water/water/water-planning-strategies/wetlands-in-bc#:~:text=British Columbia%27s wetlands currently)
939 [comprise, fish%2C birds and other wildlife.](https://www2.gov.bc.ca/gov/content/environment/air-land-water/water/water-planning-strategies/wetlands-in-bc#:~:text=British Columbia%27s wetlands currently), 2009.

940 Wutzler, T., Lucas-Moffat, A., Migliavacca, M., Knauer, J., Sickel, K., Šigut, L.,
941 Menzer, O. and Reichstein, M.: Basic and extensible post-processing of eddy
942 covariance flux data with REddyProc, *Biogeosciences*, 15(16), 5015–5030, 2018.

943 Yamasoe, M. A., Randow, C. von, Manzi, A. O., Schafer, J. S., Eck, T. F. and Holben,
944 B. N.: Effect of smoke and clouds on the transmissivity of photosynthetically active
945 radiation inside the canopy, *Atmos. Chem. Phys.*, 6(6), 1645–1656, 2006.

946 Yamasoe, M. A., DoRosário, N. M. E. and Barros, K. M. de: Downward solar global
947 irradiance at the surface in São Paulo city—The climatological effects of aerosol and
948 clouds, *J. Geophys. Res. Atmos.*, 122(1), 391–404, 2017.

949 Yu, H., Liu, S. C. and Dickinson, R. E.: Radiative effects of aerosols on the evolution
950 of the atmospheric boundary layer, *J. Geophys. Res. Atmos.*, 107(D12), AAC-3,
951 2002.

952